RESEARCH ARTICLE

Macromolecular Materials and Engineering
www.mame-journal.de

Three-Level Hierarchical 3D Network Formation and Structure Elucidation of Wet Hydrogel of Tunable-High-Strength Nanocomposites

Tzu-Yi Yu, Yun-Hsiu Tseng, Chun-Chieh Wang, Ting-Han Lin, Ming-Chung Wu, Cheng-Si Tsao, and Wei-Fang Su**

The structural characterization of wet gel state hydrogels at multi-length scales ranging from nanometers to micrometers is very challenging and rarely reported. Herein, tunable high-strength nanocomposite hydrogels based on cellulose nanofibers with various cross linkers are synthesized and characterized. Synchrotron tomography and small-angle X-ray scattering methods are combined to quantitatively elucidate 3D hierarchically wet gel state network structures, providing an understanding on the structure–properties relationship of hydrogels. The hierarchical 3D network of wet gel demonstrates three levels of structures: 1) the bundle aggregated by cellulose nanofibers; 2) physically crosslinked bundle networks; and 3) fractal-structure agglomerates composed of aggregated network domains. The finding of fractal agglomerate structures tuned by crosslinker characteristics provides fundamental knowledge to explain a variation of several orders of magnitude of mechanical properties and reveals different formation mechanisms, opening a new and flexible prospect for wet gel state material design and processing control.

1. Introduction

Hydrogels are high water content (>90%) 3D-structured materials with tunable chemical and physical properties such as biocompatibility, biodegradation, viscosity, elasticity, plasticity, modulus, and so on. They have wide applications in drug delivery, biomedicine, cell culture, tissue engineering, food industry, and so on because of their biomimetic structure and biocompatibility.[1] Hydrogels are prepared by using natural or synthetic polymers crosslinked physically, chemically, or a combination of both.[2] A mesh or 3D network architecture is formed. Physically crosslinking is noncovalent intermolecular interactions through static charge attractions, hydrophobic interaction, or hydrophilic segment stacking. On the other hand, the chemical crosslinking arises from covalent chemical bond formation among molecules.[3] For medical and food applications, natural polymers such as polypeptide, polysaccharide, polyglucosamine, etc., are preferred due to their exceptional biocompatibility and biodegradability. However, they usually exhibit low storage moduli in high water content (>90 wt%) wet gels, less than few thousands pascal due to physical crosslinking.[4] Recently, cellulose nanofiber (CNF), the most abundant natural biopolymer available from plants has attracted a great deal of attention due to their nanometer-scale diameter, adjustable surface chemistry, high specific surface area, excellent mechanical properties, and superior stability.[1b,5] It is an ideal component to be crosslinked with biopolymer to form a high mechanical strength nanocomposite hydrogel for tissue engineering. The novel properties of nanocomposite hydrogel in its high hydrate state (≈99% water) are determined by their complex structure in which CNF is hierarchically assembled to form different network architecture.[6] The structure and behavior evolution of each component in the nanocomposite of wet state are of great interest to the scientific community. However, their structural characterization and mechanistic study in the wet gel state face unique challenges and rarely investigated.[5c,7]

Hydrogel properties hinge on the characteristics of macromolecules including their dimension, physical strength, molecular orientation, chemical composition, network mesh size

T.-Y. Yu, Y.-H. Tseng, C.-S. Tsao, W.-F. Su
Department of Materials Science and Engineering
National Taiwan University
No. 1, Sec. 4, Roosevelt Rd., Taipei 10617, Taiwan
E-mail: cstsao@iner.gov.tw; suwf@ntu.edu.tw
C.-C. Wang
National Synchrotron Radiation Research Center
101 Hsin-Ann Rd., Hsinchu Science Park, Hsinchu 30076, Taiwan
T.-H. Lin, M.-C. Wu
Department of Chemical and Materials Engineering
Chang Gung University
No.259, Wenhua 1st Rd., Guishan Dist., Taoyuan City 33302, Taiwan
C.-S. Tsao
Institute of Nuclear Energy Research
Atomic Energy Council
Executive Yuan, 1000 Wenhua Rd. Jiaan Village, Longtan District, Taoyuan City 32546, Taiwan
W.-F. Su
Department of Materials Engineering
Ming-Chi University of Technology
84 Gungjuan Rd., Taishan Dist., New Taipei City 243303, Taiwan

The ORCID identification number(s) for the author(s) of this article can be found under https://doi.org/10.1002/mame.202100871

DOI: 10.1002/mame.202100871

distribution, bond type, and cross-linking type.[1b] The ability to measure these structure parameters quantitatively at multiple length scales, especially from the nanoscale to microscale, plays a crucial role in optimizing the hydrogel functionality, understanding the control mechanism and relationship among process–structure–performance.[8] However, all of the existing characterization methods have inherent limitations in sample preparation, measurement resolution, local variation, and statistic data treatment. No single method can fully characterize the gel structure at wet state from nanoscale to microscale. Every method is challenged by the high-water-content, mesh size over the chain diameter, and dynamic properties of hydrogels. Electron microscopy (called direct method) provides the real space image with resolution up to submicron scale to nanoscale, but this technique requires dehydrated gel (dry sample) with distorted structure and misleading information.[9] The rapid cooling of cryo-SEM and cryo-TEM causes the geometry expansion or gel structural change.[7,10] On the other hand, the indirect method of X-ray and neutron scattering techniques [11] provides real space information by fitting the scattering data with established models. The sample of scattering method can be used as it is, without special preparation. It is a powerful tool to quantitatively measure the nanoscale network architecture of hydrogel.[5c,7,12]

From theoretically [8b,8c] and experimentally [12b,12d] mechanistic studies, the mesh size of network architecture of crosslinked hydrogels mainly controls the mechanical property which can be tuned by the crosslinking density, type of crosslinking, etc. A recent study proposed "intra-bundle crosslinking approach" in which the crosslinking is predominately formed among polymer chains in a bundle.[12e] Then, the bundles construct into the network architecture through physical or dynamical crosslinking. The diameter of bundles governs the mechanical property instead of network mesh size. These effective crosslinks enable the formation of gel with open porous structure which is critical for many biomedical applications. In contrast, chemical or statistical crosslinking (by covalent bonding) often results in the gel with a small mesh size which is unfavorable in 3D cell culture. However, we find that both bundle diameter and mesh size control the mechanical properties of our novel high strength nanocomposite hydrogel (described below). The mesh size and bundle/or polymer chain diameter of wet hydrogels could be uniquely measured by small-angle X-ray scattering (SAXS) method.

The hydrogels are prepared by anionic CNF cross-linked with three types of cationic linkers: 1) calcium chloride; 2) poly-L-lysine (PLL); and 3) poly L-lysine-random-L-glutamic acid (PLLGA). The PLL is a polypeptide ionomer promoting cell adhesion in vitro cell culture.[13] The PLLGA, is an ionomer of random copolymer comprised of 80% of lysine and 20% of glutamic acid in molar ratio. The glutamic acid is a neuron stimulant which is designed in the PLLGA for neuron tissue engineering application.[14] The polypeptide crosslinked CNF is a very novel and interesting biomaterial which has not been reported before. We are also surprised to observe polypeptide crosslinked CNF can exhibit several order higher storage modulus than that of salt crosslinked CNF. To uncover the reasons behind this discovery, we systematically investigate and elucidate the structure of a wet gel in-depth and a three level hierarchical 3D network formation mechanism is proposed.

By combination of synchrotron SAXS and X-ray 3D tomography, we elucidate the 3D real-space structure of wet gel from few nanometers to several micrometers. The 3D tomography shows how a 3D fractal-like and swollen network structure in the environment of water is constructed by 2D network-structure domains with the size of tens of nanometers. Meanwhile, the detailed structure parameters of its basic network domain in the wet gel state, such as CNF diameter, bundle diameter, and dynamical mesh size (the 1st- and 2nd-level structures), is revealed by SAXS. The variation and control of larger-scale 3D fractal-like structure (the 3rd-level structure: agglomerate) revealed by tomography is related to the dynamical mesh size of its basic network domains tuned by the characteristics of crosslinkers. In contrast, the freeze-dried SEM image provides the limited information (non-swollen state) because of lack of water. The new finding provides the insight for the first time into a comprehensive relationship between structure parameters and mechanical property with a variation of several orders of magnitude. Different formation mechanisms tuned by crosslinker characteristics are revealed, opening a new and flexible prospect for wet-gel material design and control.

2. Results and Discussion

Both PLL and PLLGA were synthesized by conventional ring-opening polymerization (ROP) method, shown in **Scheme 1**. The details of polypeptide synthesis and nanocomposite hydrogel preparation are described in the Experimental Section. The compositions of the selected hydrogel products were analyzed by elemental analysis. The results are shown in Table R1, Supporting Information. Within the standard deviation, the results show the compositions of the CNF-polypeptide hydrogels are the same as the combined compositions of precursor solution of CNF and polypeptide crosslinker which indicates the crosslinker in precursor solution is fully attached with CNF to form nanocomposite hydrogels. However, the CNF-$CaCl_2$ hydrogel, the amount of Ca is about half of feed concentration. The amount of $CaCl_2$ may be in excess which was removed during sample preparation. The mixture of each component listed in **Table 1** reflects the composition of their corresponding hydrogel product. The concentrations of crosslinkers are labeled as their equivalent molar charge concentration for clarity.

2.1. Storage Modulus and Water Content of CNF Nanocomposite Hydrogels

In this research, the mechanical properties of CNF nanocomposite hydrogels have been extensively studied by dynamic shear rheometer, shown in Figure R1, Supporting Information. The results show their storage moduli are not influenced by time and slightly by frequency, shows effect at a strain of more than 2%. The tensile test is commonly used in characterizing hydrogel mechanical strength. As shown in the Figure R1, Supporting Information, our CNF hydrogels can hardly bear the strain more than 2%. Thus, we cannot measure the tensile strength of our hydrogels. Many biological and synthetic bundled networks show strain-stiffening behavior which was not observed in our system.

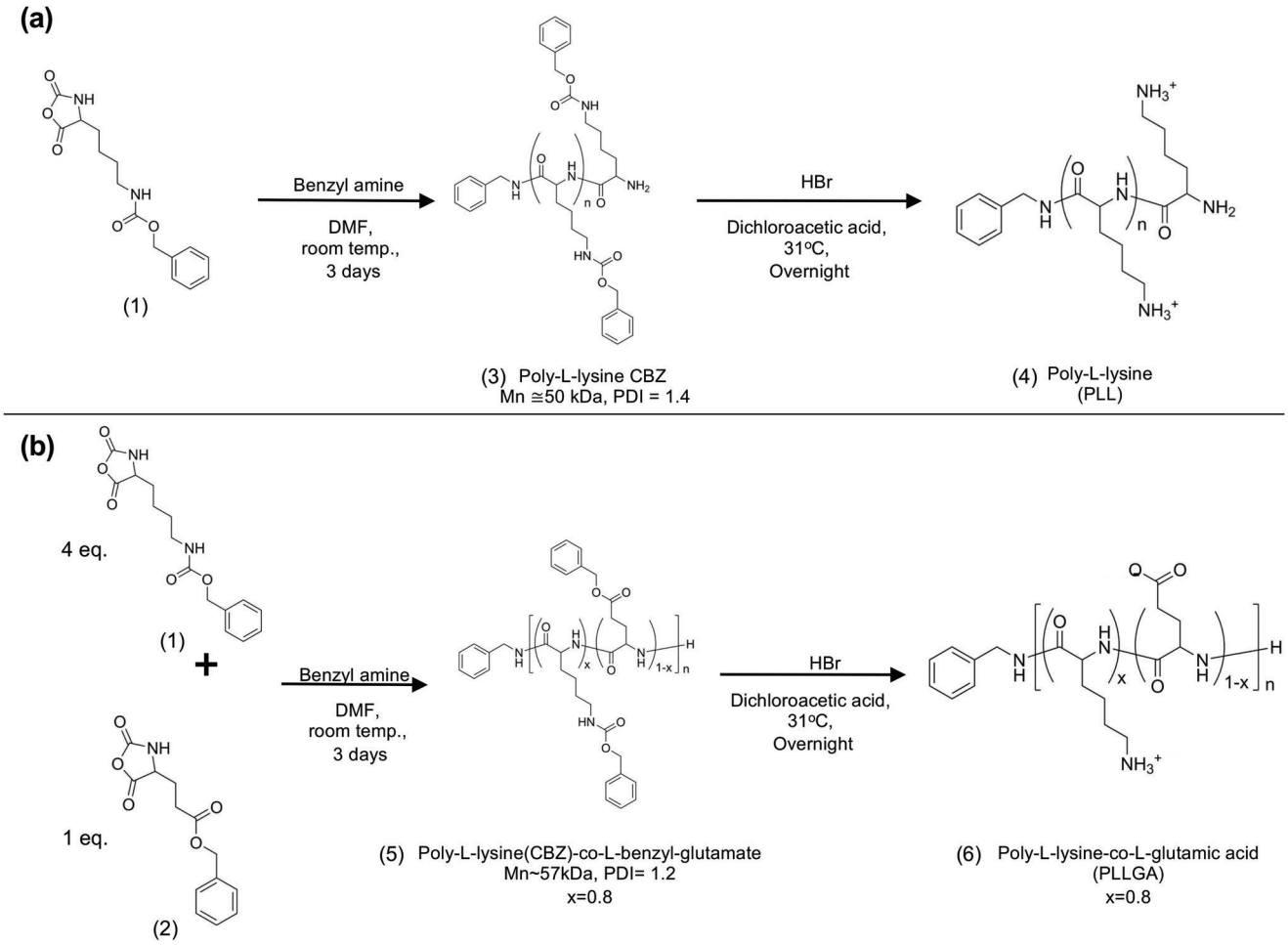

Scheme 1. Synthetic route of a) PLL and b) PLLGA.

Table 1. Compositions, structural parameters, and physical properties of CNF nanocomposite hydrogels.

Sample number	CNF [wt%]	Crosslinker		Radius [nm][b]	$I_{OZ}(0)$[c]	ξ[d] [nm]	G′ [kPa][e]	Water content [wt%]
		Type	Concentration [mM][a]					
1	1.9	$CaCl_2$	0	1.57	0	0	-	98.1
2-1	1.9	$CaCl_2$	12.5	1.91	575	55	0.20 (0.18)	99.0 (0.1)
2-2	1.9	$CaCl_2$	50	2.55	2218	56	22.15 (5.29)	98.2 (0.1)
2-3	1.9	$CaCl_2$	200	2.79	7328	83	35.90 (6.36)	97.8 (0.0)
3-1	0.6	PLL	50	2.61	68	12.4	29.75 (6.88)	98.2 (0.3)
3-2	1.2	PLL	50	2.74	60	12.6	65.94 (11.69)	97.6 (0.0)
3-3	1.9	PLL	50	2.71	90	10.7	174.70 (25.54)	96.8 (0.4)
4-1	0.6	PLLGA	50	2.59	31	7.0	34.76 (8.68)	97.2 (0.4)
4-2	1.2	PLLGA	50	2.74	59	8.0	76.75 (6.72)	96.4 (0.8)
4-3	1.9	PLLGA	50	2.78	101	9.0	173.62 (39.34)	96.4 (0.8)

[a] The concentration of crosslinker is labeled in "equivalent molar charge concentration" rather than real molar concentration; [b] The uncertainties of fitted radius and correlation length are less than 3% and 10%, respectively; [c] $I_{OZ}(0)$, a scale factor, represents the volume fraction of the CNF network; [d] ξ stands for dynamic correlation length, or mesh size, of CNF network; and [e] $n = 3$ for rheology measurement. The standard deviation of storage modulus and water content are labeled in brackets.

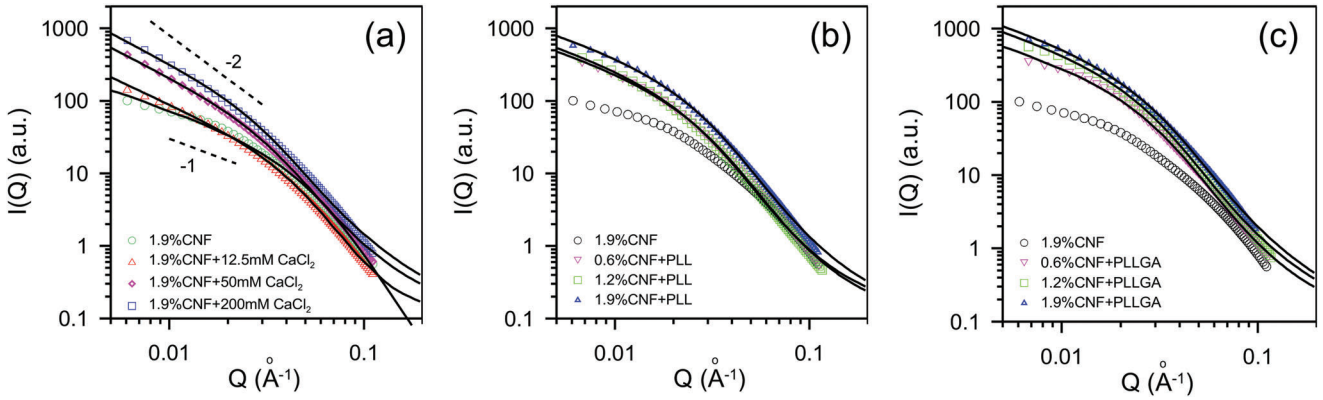

Figure 1. SAXS profiles of various wet hydrogels prepared by a) 1.9 wt% of CNF crosslinked with different $CaCl_2$ concentrations (sample 1, 2-1, to 2–3), b) different weight percentages of CNF crosslinked with 50 mM PLL (sample 3-1 to 3-3), and c) different weight percentages of CNF crosslinked with 50 mM PLLGA (sample 4-1 to 4-3). The black solid curves are the model-fitted SAXS profiles. The dashed lines show the power-law scattering behaviors.

The CNF is a rigid molecule and becomes bundled naturally.[15] It is not like flexible molecules that show strain-stiffening, rubber is a typical example. The strain-stiffening effect decreases after crosslinking. Our CNF is crosslinked, it does not exhibit any strain-stiffening effect. Thus, we used storage moduli under constant strain and frequency for the mechanical strength of our hydrogels to investigate the relationship between structure and mechanical properties. The results are discussed below.

The compositions of nanocomposites and their corresponding physical properties are summarized in Table 1. The concentrations of crosslinkers are labeled as their equivalent molar charge concentration for clarity. The measured storage modulus (G′, index of mechanical property) of wet hydrogel samples range several orders of magnitude from 87 to >150 000 Pa, listed in Table 1. The use of polypeptide crosslinker significantly enhances G′ of their CNF nanocomposite hydrogel by an order higher than that of correspondent calcium-crosslinked gel. The sample 3-3 exhibits the highest G′ as compared with the literature data of physically crosslinked CNF hydrogels.[16] Furthermore, the water content of every CNF hydrogel sample in this study exceeds 90 wt%, which is extraordinarily high comparing to polymeric hydrogels with comparable G′.[17] For these intriguing results, we further investigate the details of network structures and formation mechanism of these CNF nanocomposite hydrogels in wet gel state.

2.2. Structural Characterization by SAXS and Correlation to Mechanical Property

The SAXS profiles of pristine CNF suspension, sample 1, and CNF-$CaCl_2$ hydrogels, samples 2-1, 2-2, 2–3, are shown in **Figure 1**a. The SAXS profile of the pure CNF suspension has the power-law scattering behavior ($I(Q) \propto Q^{\alpha}$) with the exponent of −1 in the middle-Q region from 0.01 to 0.025 $Å^{-1}$ (indicated by the dashed line), signifying the characteristics of long-rod particle.[11a,18] According to literature, the SAXS profile of CNF solution with a shoulder at 0.02 $Å^{-1}$ (related to the radius of cylinder) can be modelled by the long cylinder form factor having a Schulz distribution in radius as shown in the following: [11a,18]

$$I_{\mathrm{CNF}}(Q) = \frac{\eta}{V_p}\,\delta\rho 2 \int_0^{\frac{\pi}{2}} \left[2\left(\pi r^2 L\right) f(r) j_0\left(\frac{QL}{2}\cos\alpha\right) \times \frac{J_1\left(Qr\sin\alpha\right)}{Qr\sin\alpha} \right]^2 \sin\alpha\, d\alpha dr \quad (1)$$

where V_p is the volume fraction of CNF, $\Delta\rho$ is the difference in scattering length density between the CNF and water, $f(r)$ is the Schulz distribution of the radius and V_p is the mean volume of CNF. j_0 and J_1 are the spherical and the first-order Bessel functions, respectively. The polydispersity of the Schulz distribution is defined by $\sigma / R_{\mathrm{mean}}$, σ is the variance of distribution, R_{mean} is the mean radius.[19] The integral over α is the average of the form factors with all orientations respect to the scattering vector Q. The SAXS intensity in the high-Q region is mainly contributed by radius, r, of matter. The determined mean radius is 1.57 nm, close to the radius of reported single CNF (1–2 nm).[20] The wide polydispersity of 0.6 is due to the ease of self-assembly of high aspect-ratio of CNF. This SAXS profile demonstrates thin-rod-like CNF is well dispersed in water due to the presence of hydroxyl (–OH) and carboxylic anion (–COO–) on CNF synthesized by TEMPO method.[21]

The upturn intensity in the low-Q region (0.006–0.03 $Å^{-1}$) of SAXS profile of this CNF-based hydrogel increases with the increase of $CaCl_2$ concentration, exhibiting the power-law scattering of the exponent of −2 (indicated by the dashed line). This behavior reveals the formation and evolution of gel network architecture, which can be described by Ornstein–Zernike equation and characterized by dynamic correlation length (i.e., mesh size between CNFs) of the network.[7,12b,12c,12e,22] Then, the SAXS profiles of hydrogel structure can be expressed as the following:[12b,12e,22]

$$I(Q) = I_{\mathrm{CNF}}(Q) + I_{\mathrm{bundle}}(Q) + I_{\mathrm{network}}(Q) \quad (2)$$

$$I(Q) = I_{\mathrm{bundle}}(Q) + \frac{I_{\mathrm{OZ}}(0)}{1 + Q^2\xi^2} \quad (3)$$

where $I_{\mathrm{OZ}}(0)$, a scale factor, is related to the volume fraction of the CNF network.[12a,23] In the Equation (2), the intensity is

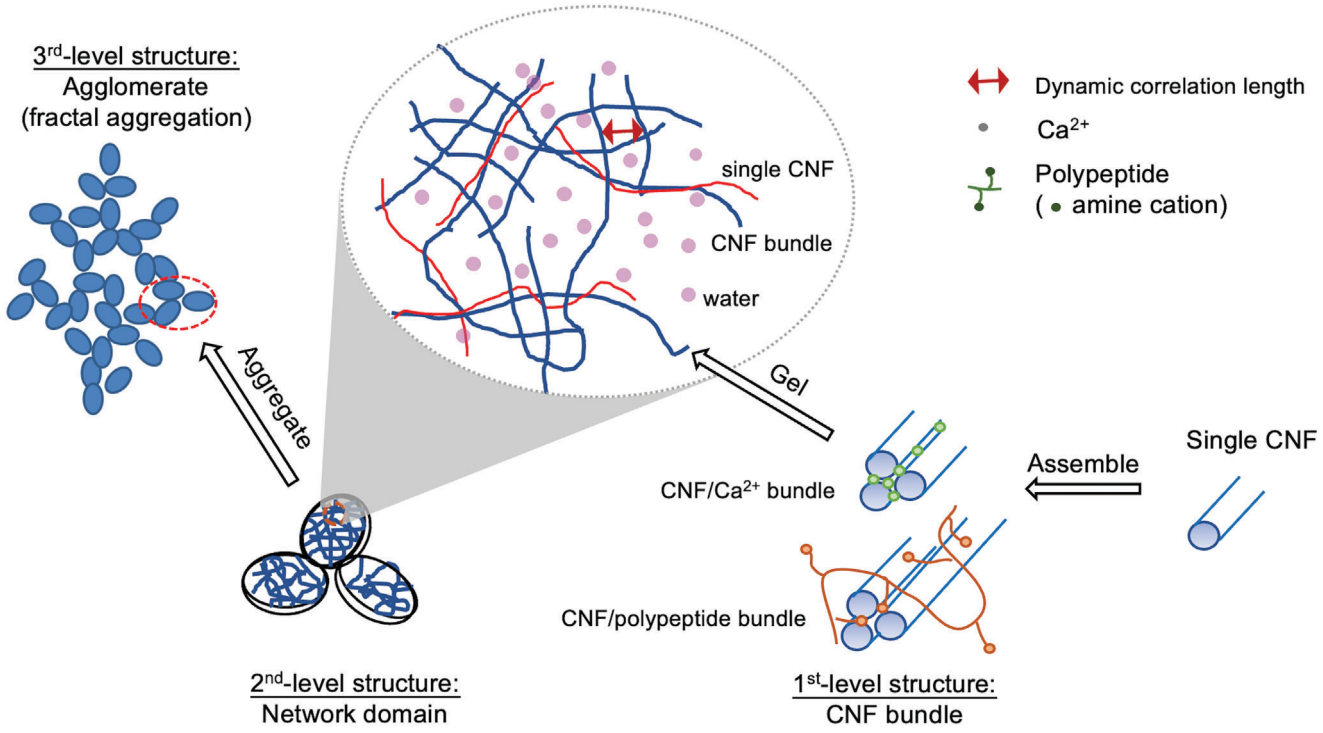

Figure 2. Schematic representation of 1) single CNFs assemble into the bundle (the 1st-level structure); 2) bundles crosslinked into the network architecture which is filled up by water molecules (the 2nd-level structure); and 3) network domain used as a basic unit to form fractal aggregation into agglomerate (the 3rd-level structure).

dominated by the signal of bundles and their radius distribution. The third term is the scattering contribution of network with a dynamic correlation length, ξ. The SAXS profiles of the CNF-$CaCl_2$ hydrogels can be fitted well by Equation (3), as shown in Figure 1a. The increase of fitted radius (Table 1) with $CaCl_2$ concentration reveals the evolution of CNF bundle from single CNF through the intra-bundle crosslinker of $CaCl_2$, predominantly located between CNFs inside a bundle, or, hidden inside the bundle. This quantitative analysis provides the evidence of the intra-bundle crosslinking characteristic.[12e] Though the determined dynamic correlation lengths ξ of 56–83 nm (Table 1) are not sensitive to the concentration of $CaCl_2$ linker, the determined $I_{OZ}(0)$ value reflects the variation of crosslinker concentration. The large variation of the corresponding storage modulus from 88 to 31 390 Pa can be attributed to the bundle radius as well as the $I_{OZ}(0)$ (relative volume fraction of bundled network). Thus, for CNF-$CaCl_2$ hydrogels, the bundle radius tuned by the crosslinker concentration is the main governing factor of the mechanical property. The increase of bundle radius stiffens the bundled architecture. The schematic representation of the bundled network architecture swollen by water is shown in **Figure 2**.

The SAXS profiles of sample 3-1 to 3-3 with the fixed 50 mM PLL as the crosslinker are shown in Figure 1b. The SAXS profiles of sample 4-1 to 4-3 with the fixed 50 mM PLLGA as crosslinker are shown in Figure 1c. The SAXS profiles of CNF-PLL and CNF-PLLGA hydrogels can be fitted well by Equation (3) with the results shown in Table 1. The bundle radius grows from ≈2.6 to 2.78 nm with increasing the CNF concentration regardless the type of polypeptide crosslinker. The determined dynamic correlation lengths ξ of 7–12 nm are not sensitive to the CNF concentration. The distinctively short correlation length ξ may be related to the abundant hydrogen bonds presenting in the hydrogel crosslinked with polypeptide whereas it is absent in the Ca^{2+} system.[24] Though CNF hydrogel crosslinked by PLLGA exhibits slightly decreased mesh size (≈7 nm) comparing to the one by PLL, it has no statistical difference on the bundle formation and the mechanical properties of their CNF hydrogels. It indicates the features of CNF-polypeptide nanocomposite hydrogel are mainly determined by the CNF concentration rather than the polypeptide constituents.

According to the extremely large difference in mechanical property caused by the characteristics of crosslinker, two types of gel network formation are revealed according to the results of SAXS analysis. They are correlated well with the mechanical property. The CNF-$CaCl_2$ is denoted as Type I hydrogel which has the large dynamic correlation length of 56–83 nm. The storage modulus ranging from 88 to 31 390 Pa is mainly tuned by the bundle radius as well as volume fraction of bundled network, which is represented by $I_{OZ}(0)$. The CNF-PLL and CNF-PLLGA are denoted as Type II hydrogels which have the short dynamic correlation length of 7–12 nm, exhibiting the storage modulus (ranging from 39 220 to 156 700 Pa) several-times higher than that of Type I. Apparently, the storage modulus of CNF-polypeptide hydrogels is mainly tuned by their mesh size. The bundle radius is a minor control factor in the Type II. Remarkably, the order of $I_{OZ}(0)$ value (or relative volume fraction) of Type II is much smaller than that of the Type I. The reason is that the short mesh size makes the network with dense

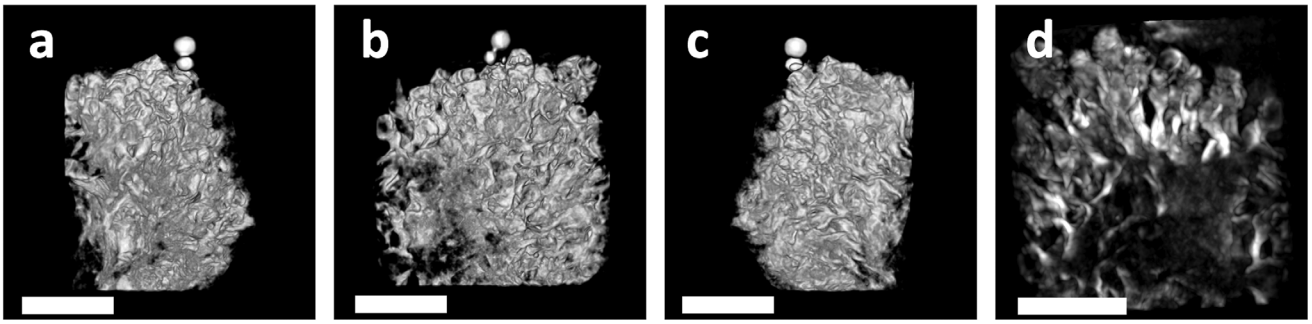

Figure 3. Snapshots of 3D tomography of 1.9 wt%-CNF+200 mM-$CaCl_2$ (sample 2–3) wet gel rotating at a) 0°, b) 90°, and c) 180° about the central axis lying on the paper. d) A slice-section of 1.9 wt%-CNF+200 mM-$CaCl_2$ (sample 2–3) from 3D model elucidating the fractal structure of agglomerate (scale bar = 6 μm). Because Ca has higher electron density than C, O, and H, the 3D tomography of CNF-$CaCl_2$ hydrogel exhibits strong contrast despite the absence of ruthenium oxide active aromatic functional groups.

structure internally, leading to the small volume fraction of total number of network domains (more discussion in Section 2.3).

Zachary K. Zander et al. demonstrated PEG-based hydrogels with the storage moduli of 20 000–28 000 Pa which had a mesh size of ≈10 nm.[12d] The other SAXS studies on the various hydrogel systems show their correlation length ranging from 3 to 6 nm.[7] However, their studies of the correlation length did not consider the influence of bundle formation. On the other hand, the study on the bundled hydrogels did not include the effect of the dynamic correlation length on mechanical property.[12e] The present study integrates the bundle radius and dynamic correlation length (mesh size) into more comprehensive relationship with mechanical property, which is reported for the first time.

The presence of chemical correlation length (or chemical linking) and dynamic correlation length (physical linking) is determined by the different power-law behaviors of SAXS profiles. The chemical correlation length is characterized by the power-law behavior of the exponent of −4. The dynamic correlation length is characterized by the power-law behavior of the exponent of −2. Basically, the exponent (or slope) of power-law behavior in the low-Q region of all measured SAXS profile is −2 in our system. Therefore, our network is dominated by physical crosslinking rather than covalently chemical crosslinking as we designed.

2.3. 3D Hierarchical Structure Determined by Synchrotron Tomography

Aforementioned, the SAXS technique reveals the bundle structure aggregated by CNFs (as the 1st-level structure; <6 nm in size) with the dynamic correlation length (with tens of nanometers) characterizing the internal structure of bundled network (as the 2nd-level structure). The measured low-Q range of SAXS limits the determined structure above 120 nm, thus the 2nd-level network domain size cannot be obtained by SAXS. For linking the probing range which cannot be attained by SAXS measurement, the synchrotron 3D tomography as real-space technique for the wet-state hydrogels was conducted here. **Figure 3**a–c shows the 3D tomography of sample 2–3, one of CNF-$CaCl_2$ hydrogels, at every 90°, demonstrating the micrometer-scale fractal-like structure. The primary domain (basic unit) constructing this micrometer-scale 3D network is the curved surface with wrinkle fringe of 1560 ± 362 nm in size (counting statistics in, Figure S2, Supporting Information). It can be speculated that the primary curved surface domain is the 2nd-level network domain, as shown in Figure 2. As discussed before, the 2nd-level network domain causes the power-law behavior (i.e., an evidence of fractal structure) in the SAXS profiles, signifying the 2D-like structure with the internal network of the mass fractal dimension of ≈2. The characteristic of fractal structure is the self-similarity at the multi-length-scale.[5,10c,25] This micrometer-scale 3D network is swollen by the occupied water molecules and is considered as the 3rd-level of agglomerate with an estimated size of ≈25 μm. The primary curve-surface-like network domains are densely developed along X–Y–Z directions by the means of fractal packing (2D-like) within the agglomerate, as shown in Figure 3d. Basically, this fractal packing with primary network domains is uniformly and densely distributed within the agglomerate. The corresponding fractal dimension of the packed network in the agglomerate is close to 3.

Figure 4a–c shows the 3D tomography of the sample 4-3, one of CNF-PLLGA hydrogels, also demonstrating the micrometer-scale fractal-like structure. In contrast to the sample 2–3, the primary network domain is much smaller and has the sheet shape of 560 ± 176 nm in size. The reason is that the dynamic correlation length of CNF-PLLGA hydrogel is several times smaller than that of CNF-$CaCl_2$ hydrogel, leading to the stiffened and small sheet domain with internally dense network. Meanwhile, the large correlation length of CNF-$CaCl_2$ hydrogel makes the large network domain with wrinkle fringe. The 2nd-level network domains are heterogeneously developed within the 3rd-level of agglomerate. At a certain orientation, the internal structure of agglomerate shows the full 3D packing arrangement of the 2nd-level network domains, as shown in Figure 4d. The corresponding fractal dimension of the packed network in the agglomerate would be close to 2. This remarkable structural (or spatial) arrangement may be closely related to the sheet-like shape and size of 2nd-level network domain. Most of space within the agglomerate is occupied by water molecules. The plane-like and heterogeneously fractal packing of smaller and stiffened domains may be the cause of increased mechanical strength by several times compared to the agglomerate of high

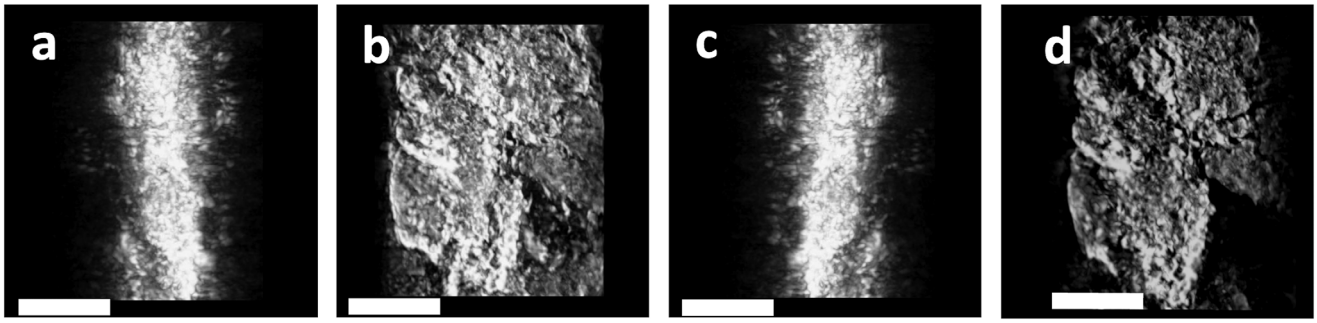

Figure 4. Snapshots of 3D tomography of the 1.9 wt%-CNF+50 mM-PLLGA (sample 4-3) wet-gel rotating with a) 0°, b) 90°, and c) 180° about the central axis lying on the paper. d) A slice-section of 1.9 wt%-CNF+50 mM-PLLGA (sample 4-3) from 3D model elucidates the fractal structure of agglomerate (scale bar = 6 μm). Since there is no aromatic functional group in both PLL and CNF, the 3D tomography of CNF-PLL hydrogel has relatively low contrast due to the image enhancing agent, ruthenium oxide, cannot be absorbed on them.

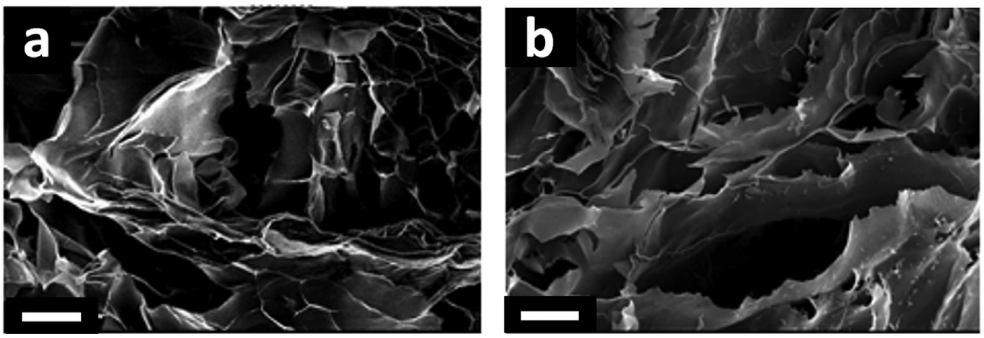

Figure 5. SEM images of freeze-dried samples a) 1.9 wt%-CNF+200 mM-$CaCl_2$ hydrogel (sample 2–3) and b) the 1.9 wt%-CNF+50 mM-PLL hydrogel (sample 4-3). The scale bar is 50 μm.

fractal dimension. The freeze-dried SEM images of two hydrogels, sample 2–3 and sample 4-3, are shown in **Figure 5**, showing very limited structural information. The image from TEM and atomic force microscope of the dried samples is also very limited (Figure S1, Supporting Information).

The substantial structure difference of the 3rd-level agglomerate is mainly caused by dynamic correlation length of primary network domain, which is connected to the two types of the 2nd-level network domain architecture (Type I and Type II) induced by the characteristics of crosslinker as previously discussed. Though the chain diameter or mesh size of network at the nanoscale is correlated to the mechanical property, there exists a puzzle of why a variation of few nanometers in the structure parameters can induce the variation of several order of magnitude in storage modulus (from 100 Pa up to 170 000 Pa). The 3rd-level swollen-state agglomerate structure reveals more structural parameters and freedom (such as size and geometry of basic domain, fractal dimension, spatial distribution, etc.) with a much broad-length scale from nanometers to micrometers scale which cause the variation of several orders of magnitude in property. Also, the hierarchical structure of CNF hydrogel explains the high storage modulus and water content; the densely packed network domains (the 2nd-level) provide mechanical support. Meanwhile, the agglomerate (the 3rd-level) of network domains leaves plenty of space filled with water molecules, providing the flexible space for molecule transport/diffusion in wet environment.

3. Conclusion

The tunable-high-strength nanocomposite hydrogels were prepared by controlling the types of crosslinker and cellulose nanofiber (CNF) concentration. The magnitude of storage modulus is varied in several orders from 100 to ≈170 000 Pa which is the highest value as compared to the literature data. We combine the synchrotron tomography and SAXS method to quantitatively present the 3D hierarchically wet gel state (swollen) network structures from nanoscale to microscale which is a breakthrough compared to the current characterization methods. The revealed hierarchical 3D network of wet gel can be divided to: 1) the 1st-level structure: the CNF bundle assembled by CNF; 2) the 2nd-level structure: physically crosslinked bundle network, characterized by mesh size and network domain; and 3) the 3rd-level structure: fractal-structure agglomerate composed of aggregated network domains. The characteristics of network domain architecture can induce vast differences in agglomerate structures, leading to different formation mechanism and mechanical properties. The quantitative study (CNF diameter, bundle diameter, and dynamical mesh size) provides the insight into an integral relationship between structure and property of wet gel. The newly-found fractal agglomerate structure offers more comprehensive parameters (such as size and geometry of basic domain, fractal dimension, spatial distribution, etc.) and freedom at the multi-length scales. These understandings shed light on designing new

gel-state materials with balanced mechanical strength and water content, which are vital to their biomedical applications as cell-culture substrates in tissue engineering or implanted scaffold in regenerative medicine.

4. Experimental Section

General Statement: Triphosgene (330 752, 98%), benzyl amine (185 701, 99%), hydrobromic acid solution (18 735, 33 wt% in acetic acid; 244 260, 47 wt% in water), L-glutamate(bz)-OH (49 510, ≥99.0%), L-lysine(Cbz)-OH (96 840, ≥99.0%), and all solvents were purchased from Sigma-Aldrich and used as received. CNF stands for "cellulose nanofiber", L-glutamate(bz)-OH stands for L-glutamic acid γ-benzyl ester, L-lysine(Cbz)-OH stands for N-Ɛ-carbobenzyloxy-L-lysine, and PLL stands for poly-L-lysine, $PLL_{80}GA_{20}$ (or PLLGA) stands for poly (L-lysine(Cbz)$_{80}$-random-L-glutamate(bz)$_{20}$). CNF was the main component of the hydrogels. The CNF hydrogel crosslinked by polypeptide either PLL or PLLGA is named CNF-PLL and CNF-PLLGA respectively. Similarly, the CNF hydrogel crosslinked by $CaCl_2$ is named CNF-$CaCl_2$.

The chemical reactions of polypeptides synthesis are shown in Scheme 1, in the Results and Discussion section. The synthetic procedures of LLCbz-NCA and LBG-NCA referred to the reported procedures with some modification.[26] The polymerization was initiated with benzylamine with a monomer-initiator ratio at 100. The number of repeating units was controlled around 200. Thus, the effect of molecular weight (or number of repeating unit) of polymer was negligible on the hydrogel morphology. The purity and molecular weight of polypeptides were characterized by NMR and GPC respectively. The details of synthesis and characterization of polypeptides, cellulose source, CNF synthesis, and characterizations are described in Supporting Information.

Fabrication Procedure of CNF Nanocomposite Hydrogels: CNF hydrogels were fabricated with the dropped method according to literatures.[16a,16b] The 2 mL crosslinker solution was gently dropped in a well in 24-well plate with 1 mL CNF suspension to form the CNF hydrogels. The container was kept in still (undisturbed) in ambient (25 °C, 65%RH) overnight. Then, the supernatant of gel was removed, and the gel was immersed in DI water for another night to remove the excessive crosslinker. The volume ratio 2/1 was selected to assure that the amount of crosslinker was sufficient for the formation of CNF network. This volume ratio might vary the properties of CNF hydrogel, which is beyond the scope of the current study and will be investigated in future.

To compare the effect of crosslinker type under the same condition of gel formation, $CaCl_2$, PLL, and PLLGA aqueous solutions were prepared with an equivalent molar charge concentration. Because the calcium cation carries 2 positive charges, the equivalent molar charge concentration of calcium chloride was two-times to its actual molar concentration. The lysine repeating unit of PLL contained one positive charge, its molar charge concentration was equal to the lysine concentration in aqueous solution. Due to the opposite charge of glutamic acid and lysine, the molar charge concentration of PLLGA was calculated as 0.54 times to the combined concentration of lysine and glutamic acid in the feed of PLLGA. The details about how to calculate molar charge concentration of PLLGA are provided in the Supporting Information. For instance, $CaCl_2$, PLL, and PLLGA were prepared into 25, 50, and 92 mM aqueous solution, respectively, as 50 mM in molar charge concentration. Also, all of the crosslinker solutions were neutralized (pH = 7 ± 0.1) by either 0.1 M $NaOH_{(aq.)}$ or 0.1 M $HBr_{(aq.)}$.

General Procedure of Rheology Test: The storage moduli of CNF hydrogels were characterized by AR2000 Rheometer, TA Instrument, with an 8 mm parallel plate and 500 μm gap at 25 °C. Time scanning test recorded the storage modulus (G′) and loss modulus (G″) versus time (10 min) under 10 Hz vibration and 0.5% strain. The average modulus was calculated by three replicates of a time scanning test.

General Procedure of Water Content Characterization: The water content of hydrogels was determined from the weight difference between dried hydrogel and fresh prepared wet hydrogel. Each hydrogel sample was divided into three pieces, and their water contents were measured separately for statistical analysis. The hydrogels were dried by freeze-drying, rather than dried by vacuum oven, to prevent polypeptides from oxidation. The water content of hydrogels was calculated according to the following equation:

$$\text{Water content } (wt\%) = \left(1 - \frac{Weight_{dried\ gel}}{Weight_{wet\ gel}}\right) \times 100\% \quad (4)$$

General Procedure of Scanning Electron Microscopy (SEM): The morphology of freeze-dried hydrogel was characterized by SEM instrument of JSM6510, JEOL. The samples were frozen at −20 °C for 2 days and then dried by freeze-drying method to maintain their 3D structure. To prevent from charging during SEM imaging, the dried hydrogel sample was coated by platinum using sputter coating (20 mA, 60 s).

General Procedure of Small Angle X-ray Scattering (SAXS): The transmission SAXS data of CNF hydrogels were obtained at 23A work station in National Synchrotron Radiation Research Center, NSRRC (Taiwan). The beam energy was 15 keV, the sample-to-detector distance was 3.875 m, and the q range was from 0.005 to 0.35 $Å^{-1}$. For good SAXS results, the dehydration should be prevented, thus the hydrogel samples should be characterized within few minutes. The 2D SAXS pattern was further converted into 1D integral by software. The background transmission and scattering image were used for 1D integration.

General Procedure of Transmission X-ray Microscopy (TXM): The transmission X-ray microscope data of CNF hydrogels were obtained at the 1B work station in National Synchrotron Radiation Research Center, NSRRC (Taiwan). For the X-ray tomography study, the aqueous hydrogel sample was stained with 0.1% w/v ruthenium tetroxide in ddH_2O to enhance the contrast of hydrogel image. After 3 h of staining, the sample was washed with methanol. Hydrogel piece with a thickness of ≈14–17 μm was fixed on the holder made by polyimide tape. A 20 μL gold particle solution (400–500 nm) was added to the hydrogel as the rotation target. The sample was rotated from −75° to 75°. The 3D structure was reconstructed by computer simulation through 151 cross-section images taken per degree by TXM.

Supporting Information

Supporting Information is available from the Wiley Online Library or from the author.

Acknowledgements

Thanks to the National Synchrotron Radiation Research Center (NSRRC) for supporting small angle X-ray scattering (SAXS) and transmission X-ray microscopy (TXM) facilities. This research is granted by Ministry of Science and Technology, Taiwan, under the project number: MOST 108-2221-E-002-027-MY3.

After initial online publication, C.-S.T. was added as a corresponding author on March 9, 2022.

Conflict of Interest

The authors declare no conflict of interest.

Data Availability Statement

The data that support the findings of this study are available from the corresponding author upon reasonable request.

Keywords

hydrogels, materials science, microstructural characterization, nanocomposites, polymer materials

Received: November 23, 2021
Revised: February 6, 2022
Published online: March 6, 2022

[1] a) J. Y. Li, D. J. Mooney, *Nat. Rev. Mater.* **2016**, *1*, 16071; b) E. Prince, E. Kumacheva, *Nat. Rev. Mater.* **2019**, *4*, 99.
[2] D. Utkan, K. Ali, *Gels Handbook: Fundamentals, Properties, Applications (In 3 Volumes)*, World Scientific, Singapore **2016**.
[3] a) S. J. Buwalda, K. W. M. Boere, P. J. Dijkstra, J. Feijen, T. Vermonden, W. E. Hennink, *J. Controlled Release* **2014**, *190*, 254; b) A. Ghavaminejad, N. Ashammakhi, X. Y. Wu, A. Khademhosseini, *Small* **2020**, *16*, 2002931.
[4] A. Suzuki, S. Sasaki, *Proc. Inst. Mech. Eng., Part H* **2015**, *229*, 828.
[5] a) K. J. De France, T. Hoare, E. D. Cranston, *Chem. Mater.* **2017**, *29*, 4609; b) N. Lin, A. Dufresne, *Eur. Polym. J.* **2014**, *59*, 302; c) M. Martínez-Sanz, D. Mikkelsen, B. M. Flanagan, C. Rehm, L. De Campo, M. J. Gidley, E. P. Gilbert, *Polymer* **2016**, *105*, 449.
[6] a) T. Li, A. J. Senesi, B. Lee, *Chem. Rev.* **2016**, *116*, 11128; b) Y.-C. Lin, H.-L. Chen, T. Hashimoto, S.-A. Chen, *Macromolecules* **2016**, *49*, 7535.
[7] V. S. Raghuwanshi, G. Garnier, *Adv. Colloid Interface Sci.* **2019**, *274*, 102044.
[8] a) X. Zhao, *Soft Matter* **2014**, *10*, 672; b) Z. Liu, W. Toh, T. Y. Ng, *Int. J. Appl. Mech.* **2015**, *07*, 1530001; c) Z. Ding, Z. Liu, J. Hu, S. Swaddiwudhipong, Z. Yang, *Int. J. Solids Struct.* **2013**, *50*, 2610; d) L. Brassart, Q. Liu, Z. Suo, *J. Mech. Phys. Solids* **2016**, *96*, 48; e) L. Liu, L. Li, Y. Qing, N. Yan, Y. Wu, X. Li, C. Tian, *Polym. Chem.* **2016**, *7*, 48.
[9] L. E. Franken, K. Grünewald, E. J. Boekema, M. C. A. Stuart, *Small* **2020**, *16*, 1906198.
[10] a) Z. Kochovski, G. Chen, J. Yuan, Y. Lu, *Colloid Polym. Sci.* **2020**, *298*, 707; b) M. A. Cianfrocco, E. H. Kellogg, *J. Chem. Inf. Model.* **2020**, *60*, 2458.
[11] a) O. Glatter, O. Kratky, *Small Angle X-Ray Scattering*, Academic Press, London, New York **1982**; b) H.-C. Liao, C.-S. Tsao, T.-H. Lin, C.-M. Chuang, C.-Y. Chen, U.-S. Jeng, C.-H. Su, Y.-F. Chen, W.-F. Su, *J. Am. Chem. Soc.* **2011**, *133*, 13064; c) R. J. Roe, *Methods of X-Ray and Neutron Scattering in Polymer Science*, Oxford University Press, New York **2000**.
[12] a) T. Norisuye, N. Masui, Y. Kida, D. Ikuta, E. Kokufuta, S. Ito, S. Panyukov, M. Shibayama, *Polymer* **2002**, *43*, 5289; b) G. Ochbaum, M. Davidovich-Pinhas, R. Bitton, *Soft Matter* **2018**, *14*, 4364; c) M. Shibayama, *Polym. J.* **2010**, *43*, 18; d) Z. K. Zander, G. Hua, C. G. Wiener, B. D. Vogt, M. L. Becker, *Adv. Mater.* **2015**, *27*, 6283; e) D. C. Schoenmakers, A. E. Rowan, P. H. J. Kouwer, *Nat. Commun.* **2018**, *9*, 2172.
[13] a) X. Zhang, T. Viitala, R. Harjumäki, A. Kartal-Hodzic, J. J. Valle-Delgado, M. Österberg, *J. Colloid Interface Sci.* **2021**, *584*, 310; b) D. Mazia, G. Schatten, W. Sale, *J. Cell Biol.* **1975**, *66*, 198; c) E. Yavin, Z. Yavin, *J. Cell Biol.* **1974**, *62*, 540.
[14] C.-Y. Lin, S.-C. Luo, J.-S. Yu, T.-C. Chen, W.-F. Su, *ACS Appl. Bio Mater.* **2018**, *2*, 518.
[15] W. Chen, Q. Li, J. Cao, Y. Liu, J. Li, J. Zhang, S. Luo, H. Yu, *Carbohydr. Polym.* **2015**, *117*, 950.
[16] a) A. Basu, J. Lindh, E. Ålander, M. Strømme, N. Ferraz, *Carbohydr. Polym.* **2017**, *174*, 299; b) N. Masruchin, B.-D. Park, V. Causin, I. C. Um, *Cellulose* **2015**, *22*, 1993; c) K.-C. Cheng, C.-F. Huang, Y. Wei, S.-h. Hsu, *NPG Asia Mater.* **2019**, *11*, 25; d) J. R. Mckee, S. Hietala, J. Seitsonen, J. Laine, E. Kontturi, O. Ikkala, *ACS Macro Lett.* **2014**, *3*, 266; e) J. Yang, X. Zhang, M. Ma, F. Xu, *ACS Macro Lett.* **2015**, *4*, 829; f) H. Dong, J. F. Snyder, K. S. Williams, J. W. Andzelm, *Biomacromolecules* **2013**, *14*, 3338.
[17] J. Cauich-Rodriguez, *Biomaterials* **1996**, *17*, 2259.
[18] Y. Su, C. Burger, B. S. Hsiao, B. Chu, *J. Appl. Crystallogr.* **2014**, *47*, 788.
[19] S. R. Kline, *J. Appl. Crystallogr.* **2006**, *39*, 895.
[20] M. Martínez-Sanz, M. J. Gidley, E. P. Gilbert, *Carbohydr. Polym.* **2015**, *125*, 120.
[21] A. Isogai, T. Saito, H. Fukuzumi, *Nanoscale* **2011**, *3*, 71.
[22] Y. Shinohara, K. Kayashima, Y. Okumura, C. Zhao, K. Ito, Y. Amemiya, *Macromolecules* **2006**, *39*, 7386.
[23] E. Geissler, F. Horkay, A.-M. Hecht, C. Rochas, P. Lindner, C. Bourgaux, G. Couarraze, *Polymer* **1997**, *38*, 15.
[24] D. Ye, P. Yang, X. Lei, D. Zhang, L. Li, C. Chang, P. Sun, L. Zhang, *Chem. Mater.* **2018**, *30*, 5175.
[25] a) D. W. Schaefer, *Science* **1989**, *243*, 1023; b) F. Pignon, A. Magnin, J.-M. Piau, B. Cabane, P. Lindner, O. Diat, *Phys. Rev. E* **1997**, *56*, 3281; c) M. Kolb, R. Botet, R. Jullien, *Phys. Rev. Lett.* **1983**, *51*, 1123.
[26] a) G. J. M. Habraken, M. Peeters, C. H. J. T. Dietz, C. E. Koning, A. Heise, *Polym. Chem.* **2010**, *1*, 514; b) G. J. M. Habraken, K. H. R. M. Wilsens, C. E. Koning, A. Heise, *Polym. Chem.* **2011**, *2*, 1322.

